Fibers and Polymers 2019, Vol.20, No.1, 120-128
DOI 10. 1007/s12221-019-8284-6

ISSN 1229-9197 (print version)
ISSN 1875-0052 (electronic version)

Preparation of MCA-SiO_2 and Its Flame Retardant Effects on Glass Fiber Reinforced Polypropylene

Jiayou Xu[1]*, Kaidan Li[1], Haiming Deng[1], Shu Lv[1], Pengkai Fang[2,3], Hu Liu[3,4], Qian Shao[2], and Zhanhu Guo[3]*

[1]*School of Chemistry & Chemical Engineering, Guangzhou University, Guangzhou 510006, China*
[2]*School of Chemistry & Chemical Engineering, College of Chemical and Environmental Engineering, Shandong University of Science and Technology, Qingdao 266590, China*
[3]*Integrated Composite Laboratory (ICL), Department of Chemical & Biomolecular Engineering, University of Tennessee, Knoxville, TN 37934, USA*
[4]*National Engineering Research Center for Advanced Polymer Processing Technology, Zhengzhou University, Zhengzhou 450002, China*

(Received April 11, 2018; Revised August 23, 2018; Accepted September 27, 2018)

Abstract: In this work, a new synergistic charring agent of melamine cyanurate-fumed silica (MCA-SiO_2) has been synthesized through the facile self-assembly process, where melamine (ME) and cyanuric acid (CA) reacted and deposited on the fumed silica in the aqueous suspension. Then GF-PP/IFR-(MCA-SiO_2) composites were prepared by melting blend of GF-PP and IFR containing MCA-SiO_2. The general properties of the resulting composites were characterized by Cone calorimeter test (CCT), scanning electron microscopy (SEM) and Fourier transform infrared spectroscopy (FT-IR) etc. Results show that the addition of SiO_2 could greatly reduced the heat release rate (HRR) of the GF-PP/IFR-MCA composites and improved the flame retardant properties during burning. When the content of SiO_2 in MCA-SiO_2 was 20 wt%, the flame retardant property of the composites reached the UL-94 V-0 rating, corresponding to a the limiting oxygen index (LOI) of 32.4 %. This enhanced flame retardant property could be attributed to the fact that the fumed silica with low thermal conductivity could prevent the heat exchange, and assist in the formation of compact and dense char during the burning.

Keywords: Polypropylene, Melamine cyanurate, Fumed silica, Intumescent flame retardant, Thermal conductivity

Introduction

Nowadays, glass fiber-reinforced polypropylene (GF-PP) nanocomposites have been widely used in household appliances, electronics, construction industry etc [1,2]. Therefore, the studies on the flame retardant properties of GF-PP has been an important topic. However, the exploration and application of the halogen-free flame retardant for GF-PP is still a great challenge due to the "candle wicking effects" of glass fibers [3]. Because glass fibers can transport the fuel from the pyrolysis of polymers to the flame by capillary action, accelerate the heat flowing back to polymers and thus cause serious self-extinguishment of PP matrix [4]. Currently, the bulk charring in condensed phase is well known as the most efficient halogen-free flame resistance mode for PP or PP composites [5-7]. Intumescent flame-retardant system (IFR) is usually composed of three components: an acid source, a char-forming agent, and a blowing agent [8]. Intumescent char layer is produced via the dehydration and charring of carbonization agents under the catalysis of acid source, and the released gases from blowing agents trigger the expansion of the forming char [9]. To improve the flame retardant property, some synergistic agents have been used in the IFR systems, such as zeolites, expandable graphite, metal chelates, and metal compounds [10-13].

Wang and co-workers studied the flame retardant long-glass-fiber reinforced PP by IFR and organic modified montmorillonite (OMMT), It appeared that the OMMT could improve the interaction of APP and CA, which produced a continuous and compact char layer to solve the flame retardant for GF-PP [14]. It seems that the OMMT could act as a physical barrier to prevent the fuel transportation from pyrolysizing polymers to the flame on the surface of GF, which is a method to improve the flame retardant for GF-PP.

Here, to solve the flame retardant for GF-PP, IFR is used to flame retardant GF-PP, which are composed of APP (acid source), PEPA (carbon source) and MCA (nitrogen source), Melamine (MCA) is a low cost, environmentally friendly and nitrogen-containing flame retardant, and has been widely used [15-17] as a nitrogen source for FIR. The commercial MCA used for the GF-PP to the flame resistance often produces a large number of melting drops due to the "candle wicking effects" of GF and limits its application. Therefore, it is necessary to modify the commercial MCA before use. Li and co-workers prepared the modified MCA by self-assembly of ME and CA in the MMT suspension [18-20]. The fumed silica with a unique three-dimensional structure and abundant hydroxyl groups on its surface possesses the characteristic of a large specific surface area,

*Corresponding author: xujiayou516@sohu.com
*Corresponding author: zguo10@utk.edu

low density, high temperature resistance and so on. Therefore, it is promising for the modification of MCA [21-23]. In addition, Fumed silica (SiO_2) is usually used as an enhancing agent in thermoplastic polymers to increase the mechanical performance of composites, such as tensile strength and toughness. Kashiwagi and coworkers have investigated the flame-retardant behavior of silica in PP [22]. Besides, the effect of the fumed silica on ethylenevinyl acetate/magnesium hydroxide blends has been reported recently [23]. Meanwhile, the hydroxyl groups on the surface of SiO_2 can react with the hydroxyl groups on the surface of the glass fiber during combustion. Therefore, we intend to use SiO_2 modified MCA to improve the flame retardant performance of MCA to GF-PP, make use of the chemical reaction between hydroxyl groups for the surface of SiO_2 and glass fiber to prevent the "candle wicking effects", finally, solve the flame retardant of GF-PP.

In this work, MCA-SiO_2 was prepared by adding the SiO_2 into the solution of MCA during during the self-assembly process, and its flame retardant performance was studied by adding it to the GF-PP composites. The effects of the SiO_2 on the flame retardant property and flame retardant mechanism of GF-PP/IFR composites are investigated via various characterization methods including FT-IR, XRD and SEM which are used to investigate whether there are chemical reactions between MCA and SiO_2, LOI, UL-94 test, CCT, SEM and TGA which are used to characterize the flame retardant effects and mechanisms of the SiO_2 on GF-PP/IFR composites.

Experimental

Materials

Melamine (ME) and cyanuric acid (CA) were purchased from Sinopharm Chemical Reagent Co. Ltd. (Shanghai, China). Fumed silica (SiO_2) with a specific surface area of 150 m^2/g and an average particle size of 14 nm was obtained from Guangzhou GBS High-Tec & Industry Co., Ltd. (Guangzhou, China). GF-PP was supplied by Foshan Magic chemical technology Co., Ltd. (Foshan, China). Ammonium polyphosphate (APP, n>1500) was obtained from Cangshan Hongchuang Flame Retardant Co., Ltd. 1-oxo-4-hydroxymethy1-2,6,7-trioxa-1-phosphabicyclo[2.2.2]octane (PEPA) was purchased from Guangzhou XiJia chemical Co., Ltd. IFR were comprised of APP, PEPA and MCA or MCA-SiO_2, in which APP used as an acid source, PEPA used as a char-forming agent and MCA or MCA-SiO_2 used as a blowing agent.

Preparation of MCA and MCA-SiO_2

Specific amount of fumed silica nanoparticles was dispersed evenly into a three-necked flask with 100 m*l* water under sonication for 30 min. Then 0.1 mol CA and 0.1105 mol ME were added into the above mixture under mechanical stirring. The mixture reacted at 95 °C for 2 h, and then the resulting MCA was dried at 120 °C for 2 h. Finally, MCA-SiO_2 with different fumed silica contents (the fumed silica account for 5, 10, 20 and 30 wt% MCA) were obtained with white powders.

Preparation of PP/IFR Composites

All samples were prepared according to the formulation in Table 1 on a two-roll mill at a temperature range of 180-185 °C for 15 min. After mixing, the samples were hot-pressed under 10 MPa for 5 min at about 185 °C into a sheet of suitable thickness and size for analysis. The schematic diagram explaining the preparation of PP/IFR composites was shown in Figure 1.

Characterization

FT-IR measurements were performed on a Nicolet IS-10, and the samples were prepared in potassium bromide pellets.

Powder X-ray diffraction (XRD) analyses were performed on a Bruker D8 Advance diffractometer with Cu-Ka radiation in the range of 5 ° to 90 ° with a scanning rate of 0.06 °/s.

Thermal conductivity was determined by IMDRY3001-I type double plate thermal conductivity meter, based on GB3399-1982 determination thermal conductivity of GF-PP/IFR-MCA and GF-PP/IFR-(MCA-SiO_2), sample size of 30×30×2 mm^3.

SEM observed on a JEOL JSM-5900LV was used to investigate the surface of char residues of the GF-PP/IFR-(MCA-SiO_2) systems after the cone calorimeter test. SEM images of the char residues were recorded after gold coating surface treatment.

Fire Test

LOI was measured using an HC-2 oxygen index instrument

Figure 1. The schematic diagram for the preparation of PP/IFR composites.

on the sheets 100×6.5×3 mm^3 according to the standard ASTM 2863/77.

UL-94 test: Vertical burning tests were carried out using a CZF-2 vertical burning test instrument with sheet dimensions of 127×12.7×3.2 mm^3 according to ASTM D-635-77.

Cone calorimeter test (CCT): The samples were exposed to a FTT Cone Calorimeter with an external heat flux of 50 kW/m^2 according to ISO 5660-1. The size of the samples was 100 mm×100 mm×3 mm^3, and the data presented in the following were averages from at least 3 tests.

Results and Discussion

Synthesis and Characterization of MCA and MCA-SiO_2

Synthesis of MCA and MCA-SiO_2

A new synergistic charring agent of melamine cyanurate (MCA)-coated fumed silica (SiO_2) nanoparticles (MCA-SiO_2) has been synthesized by the self-assembly process of ME and CA in an aqueous suspension of the fumed silica. The reaction scheme for MCA-SiO_2 is shown in Figure 2.

The influence of the added amount of SiO_2 on the yield of MCA-SiO_2 is shown in Figure 3. It was apparent that with the increasing content of SiO_2, the yield of MCA-SiO_2 was increased. The highest yield was obtained when the addition of the SiO_2 was 20 wt% of MCA. Further increasing the SiO_2 content to 30 wt% MCA, the yield of MCA slightly decreased. It appeared that the maximum content of SiO_2 in MCA-SiO_2 system was 20 wt% of MCA, likely due to that the excess amount of SiO_2 hindered the crystal growth of MCA, resulting in a lower content of MCA in MCA-30 %SiO_2.

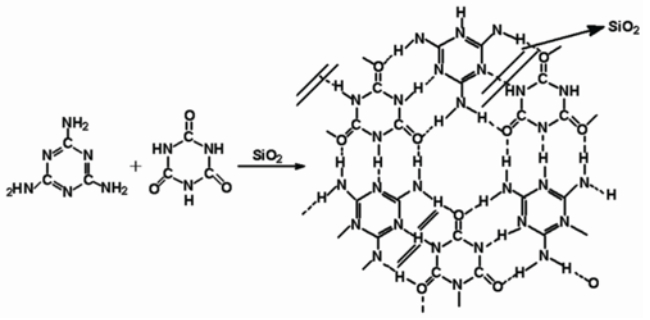

Figure 2. Schematic figures of the reaction of ME, CA and SiO_2.

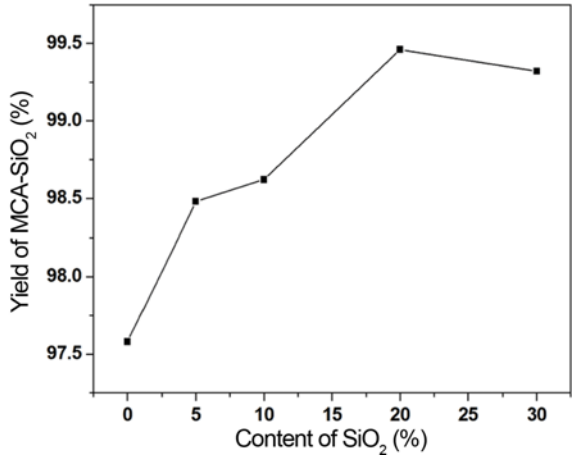

Figure 3. Effect of the added amount of SiO_2 on the yield of MCA-SiO_2.

Characterization of MCA and MCA-SiO_2

To investigate whether there were chemical reactions between MCA and SiO_2, FT-IR analysis was conducted and the results were shown in Figure 4. The peaks appeared at the 3396 and 3230 cm^{-1} could assigned to the symmetric and non-symmetric stretching vibration peaks of NH, respectively [23]. The absorption peaks at the 1788, 1743, 1668, 1448 and 1536 cm^{-1}, were correspond to the absorption characteristic

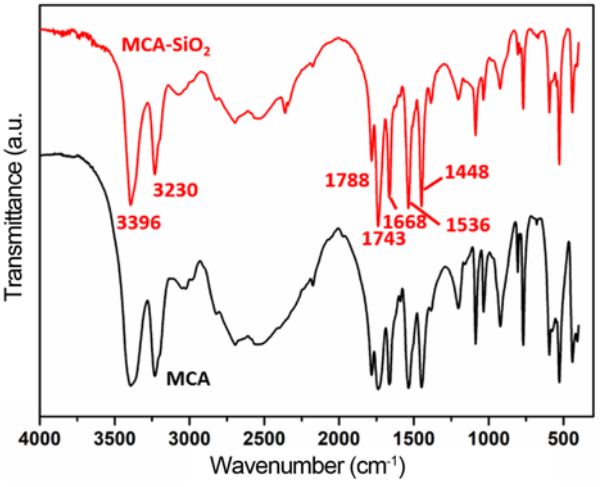

Figure 4. FTIR spectra of MCA and MCA-SiO_2.

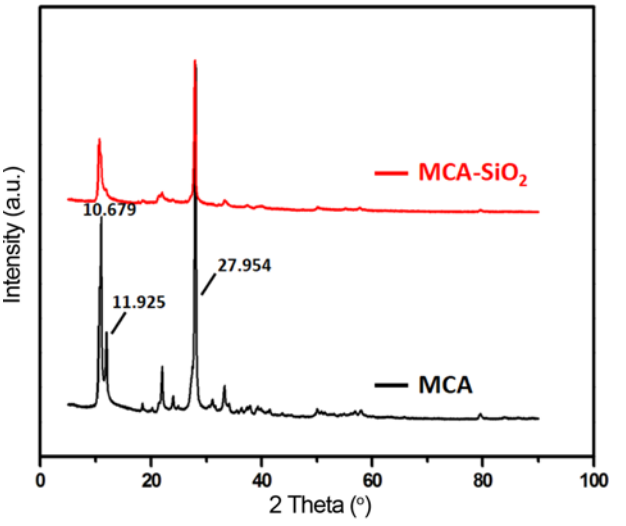

Figure 5. XRD patterns of MCA and MCA-SiO_2.

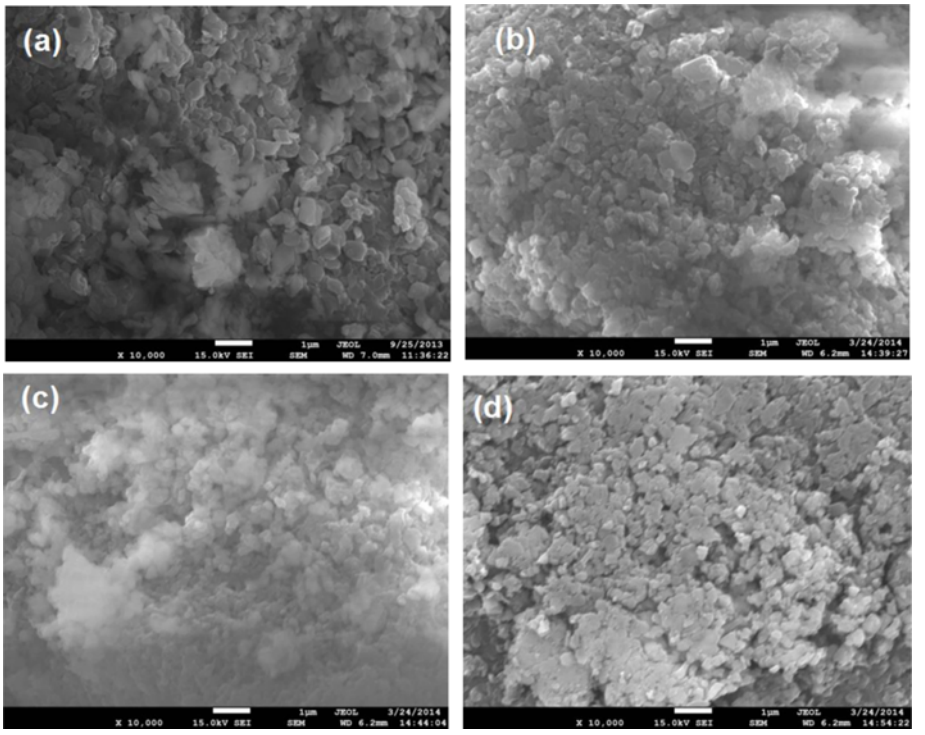

Figure 6. SEM images of (a) MCA, (b) MCA-10 %SiO_2, (c) MCA-20 %SiO_2, and (d) MCA-30 %SiO_2.

peaks of C=O bond for MCA [24]. The positions of these characteristic peaks of MCA-SiO_2 are the same as those of MCA, indicating that the infrared characteristic of MCA-SiO_2 is similar to that of MCA. XRD analysis was further conducted to study the crystal structure of MCA and MCA-SiO_2. As shown in Figure 5, the diffraction peaks for MCA and MCA-SiO_2 were observed at 2θ of 10.679 °, 11.925 ° and 27.954 °, and there were no obvious differences for MCA and MCA-SiO_2, suggesting that there are no chemical reactions occurred between MCA and SiO_2, which was consistent with previous FT-IR results.

SEM images of MCA and MCA-SiO_2 are shown in Figure 6, earlier work has shown that the synthesis of MCA was planar molecules self-assembled with ME and CA by forming a large flat hydrogen bond network [25,26]. However, in this work, the planar regularity of ME and CA was destroyed. The growth of the hydrogen bonding network was limited by introducing the fumed silica into MCA supramolecular frameworks. It can be seen from Figure 6(b), Figure 6(c) and Figure 6(d) that the size of MCA-SiO_2 particles became smaller compared with that of pure MCA when the fumed silica was added into this system, and some capsule-shaped particles appeared, which could be explained by the coating effect of MCA on SiO_2.

Thermal Stability of MCA and MCA-SiO_2

Figure 7 shows the TGA curves for MCA and MCA-SiO_2. The charred residues of MCA, MCA-10 %SiO_2, MCA-20 %SiO_2 and MCA-30 %SiO_2 at 800 °C was 0.36 %, 7.79 %, 20.2 % and 14.6 %, respectively. The fumed silica acting as a heat resistant barrier were fixed in the interlayer of the decomposed products of MCA, thus increased the weight of the char residue. The added suitable amount of SiO_2 nanoparticles in MCA-SiO_2 was 20 wt%. It appeared that the excessive amounts of SiO_2 decreased the char residue of MCA-SiO_2 due to the lower content of MCA for MCA-30 %SiO_2 sample.

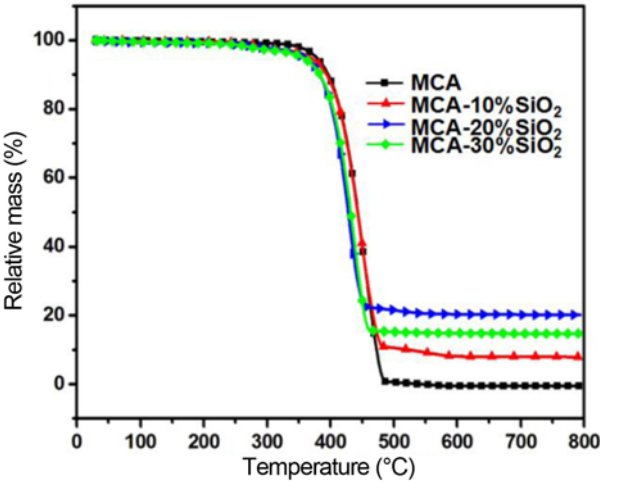

Figure 7. TGA of MCA and MCA-SiO_2 under a flow of air.

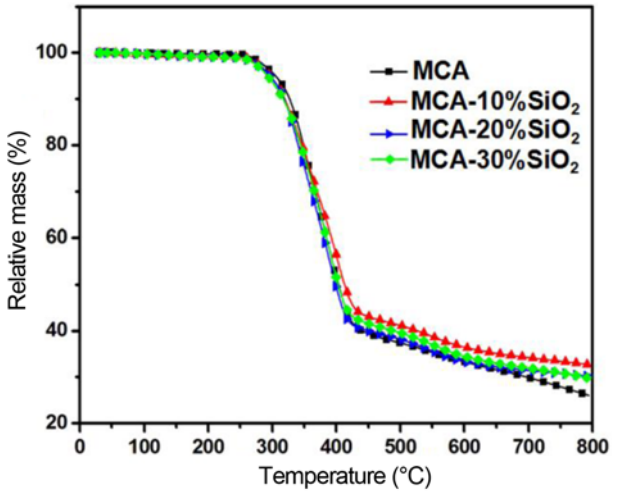

Figure 8. TGA of GF-PP/IFR-MCA and GF-PP/IFR-(MCA-SiO_2) composites.

Thermal Stability of GF-PP/IFR Composites

Figure 8 shows the TGA curves for the GF-PP/IFR-MCA and GF-PP/IFR-(MCA-SiO_2) composites. It was worth noting that their thermal decomposition profile were almost the same in the testing temperature range, thus the influence of SiO_2 addition on the thermal decomposition properties of GF-PP/IFR-(MCA-SiO_2) composites was negligible.

Flame Retardancy

Effects of the fumed silica nanoparticles on the flame retardant properties of GF-PP/IFR-MCA composites were studied and the results are shown in Table 1. With the increasing content of the fumed silica in MCA-SiO_2, the flame retardant properties of the GF-PP/IFR-(MCA-SiO_2) composites increased. When the SiO_2 content in the MCA-SiO_2 was 20 wt%, the LOI of the GF-PP/IFR-(MCA-SiO_2) nanocomposites was 32.4 %, corresponding to a flame retardant performance of UL-94V-0 rating. With the further increase of SiO_2 in the MCA-SiO_2, the LOI of GF-PP/IFR-MCA system decreased from 32.4 % to 29.4 % and the flame retardant property was also decreased from UL-94V-0 rating to UL-94V-2 rating, which was consistent with their thermal stability analysis.

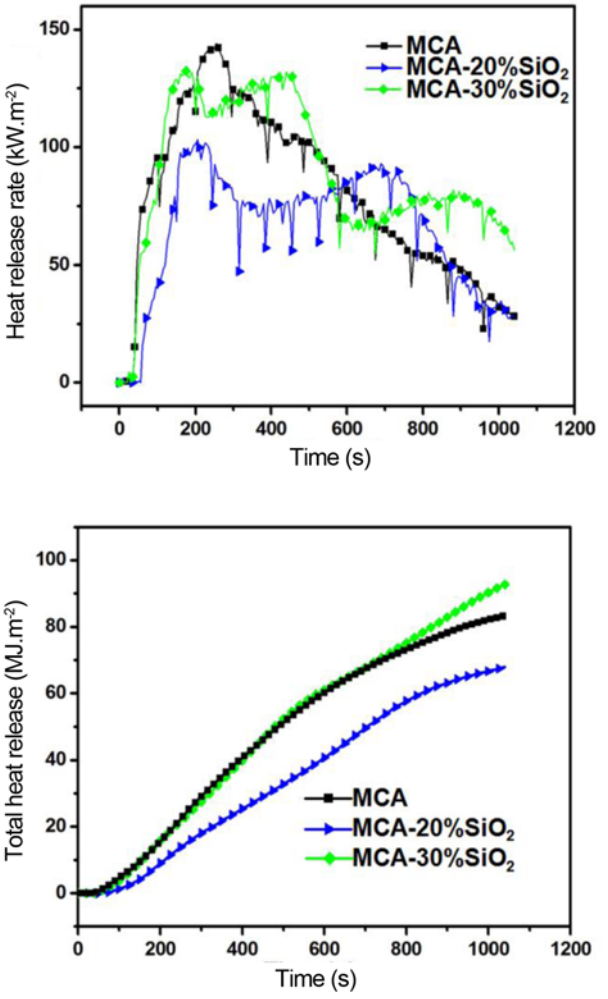

Figure 9. (a) HRR curves of GF-PP/IFR-MCA and GF-PP/IFR-(MCA-SiO_2) composites and (b) THR curves of GF-PP/IFR-MCA and GF-PP/IFR-(MCA-SiO_2) composites.

CCT is a widely used tool for evaluating combustion behaviors of various materials under real-world fire conditions [27,28]. Heat release rate (HRR) as shown in Figure 9(a) and total heat release (THR) as shown in Figure 9(b) curves for

Table 1. Effect of different content of SiO_2 on the flame retardant property of GF-PP/IFR samples

Sample	Composition	LOI (%)	UL-94			
			Dripping	Burning time (s)		Rank
				t_1	t_2	
1	GF-PP/IFR-MCA	26.8	Yes	13	24	V-2
2	GF-PP/IFR-(MCA-5 %SiO_2)	27.3	Yes	7.5	28	V-2
3	GF-PP/IFR-(MCA-10 %SiO_2)	26.4	Yes	18	22	V-2
4	GF-PP/IFR-(MCA-20 %SiO_2)	32.4	No	2	4	V-0
5	GF-PP/IFR-(MCA-30 %SiO_2)	29.4	No	4.5	24	V-2

the GF-PP/IFR-MCA and the GF-PP/IFR-(MCA-SiO_2) nanocomposites. It can be seen that the sequence of HRR of the testing samples from high to low was as follows, PP/IFR-MCA>PP/IFR-(MCA-30 %SiO_2)>PP/IFR-(MCA-20 %SiO_2), the lowest HRR of GF-PP/IFR-(MCA-20 %SiO_2) indicated that the heat release rate of GF-PP/IFR-MCA system could be reduced by the fumed silica. The slope of the THR curve was assumed to be representative of fire spread [29]. It was obvious that the flame spread of GF-PP/IFR-(MCA-20 %SiO_2) sample was comparatively low. Therefore, the optimal content of SiO_2 in MCA-SiO_2 was 20 %, this phenomenon was related to the property of the fumed silica, the charred residue, and the structure of the char layer. The flame retardant mechanism of the fumed silica on GF-PP/IFR-MCA was further investigated in following section.

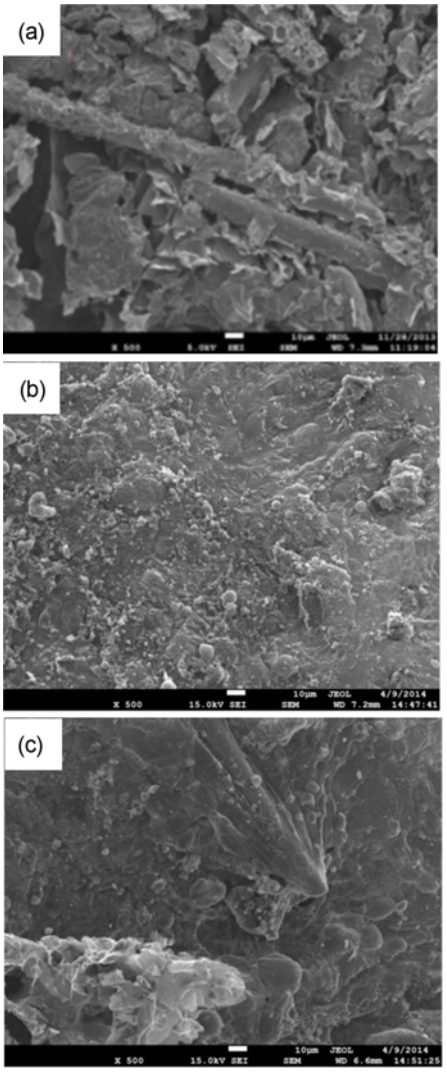

Figure 10. SEM images of the char layer for (a) GF-PP/IFR-MCA, (b) GF-PP/IFR-(MCA-20 %SiO_2), and (c) GF-PP/IFR-(MCA-30 %SiO_2) composite.

Flame Retardant Mechanism

Morphology of Charred Layers from PP/IFR Composites

Figure 10 shows the SEM images of the intumescent charred layers from the GF-PP/IFR-MCA, GF-PP/IFR-(MCA-20 %SiO_2) and GF-PP/IFR-(MCA-30 %SiO_2) samples after UL-94 test. From Figure 10(a), there were many holes, crevices and bare glass fibers, exhibited on the char surface of GF-PP/IFR-MCA. Therefore, the heat and flammable volatiles could penetrate the char layer into the flame zone during burning. However, the char layers of the GF-PP/IFR-(MCA-20 %SiO_2) sample was more compact and smooth without cracks than that of the GF-PP/IFR-MCA sample, which could effectively limit the heat and mass transfer between polymer and flame. The char layer of the GF-PP/IFR-(MCA-30 %SiO_2) sample seen in Figure 10(c) was rather coarse. The glass fiber seemed not coated. Although the char layer was more smooth than that of in Figure 10(a), and the compactness and completeness of the char layer is inadequate when compared with Figure 10(b). When a suitable amount of fumed silica forms compact charred layers, it not only prevented the heat exchange but also acted as a barrier that could prevent the decomposed volatile products from migrating onto the sample surface.

Effects of the Fumed Silica on the Thermal Conductivity of the GF-PP/IFR Composites

Figure 11 shows the effects of the fumed silica on the thermal conductivity of the GF-PP/IFR-MCA comosites. It can be seen that the thermal conductivity of GF-PP/IFR-MCA first decreased and then increased with increasing the fumed silica loading. When the added amount of SiO_2 in MCA-SiO_2 system was 20 %, the thermal conductivity of GF-PP/IFR-(MCA-20 %SiO_2) reached the lowest value of 0.322 w/m·k, which was decreased by 10 % compared with that of GF-PP/IFR-MCA. The lower thermal conductivity of GF-PP/IFR-(MCA-20 %SiO_2) effectively prevented the heat

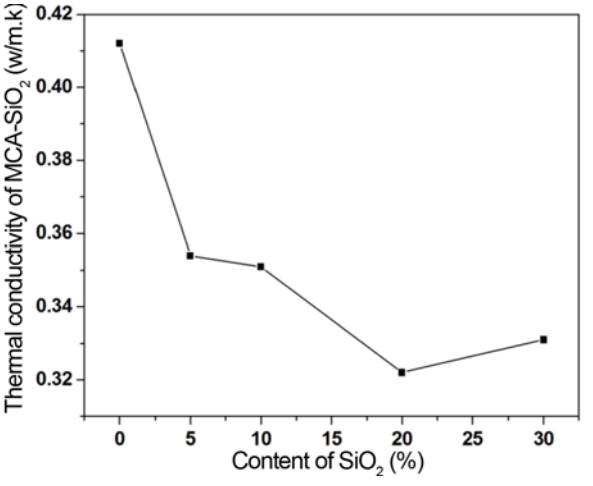

Figure 11. Effect of the fumed silica on the thermal conductivity of GF-PP/IFR composites.

transfer during the combustion process of GF-PP composites and thus improved the flame-retardant property.

FTIR Spectra of GF-PP/IFR-(MCA-SiO$_2$) Composites

In order to clarify the char-forming mechanism of the GF-PP/IFR-(MCA-SiO$_2$) composites, the FTIR spectra of the composites after heat treatment at different temperatures are shown in Figure 12. Figure 12(a) displays the FT-IR curves of the composites at 300 °C. The peaks around 3426-3141 cm^{-1}, were corresponded to the stretching vibration of -NH and -OH bonds, respectively [30], which could be explained by that the decomposition of APP at low temperature can form some polyphosphoric acid. The peaks at 2939, 1458, 1378 cm^{-1} were contributed to the -CH$_2$- bond. The strong absorption peaks at 1657 cm^{-1} was associated with -C=N, -C=O bonds in MCA, respectively. In addition, the absorption peaks of P=O bonds at 1145 and 993 cm^{-1} also existed in the FT-IR spectra, which were assigned to the bonds of PEPA. Because the maximum thermal degradation temperature of PEPA was 326 °C [31] and MCA was 440-450 °C [32]. Therefore, the PEPA and MCA exhibited better thermal stability at 300 °C.

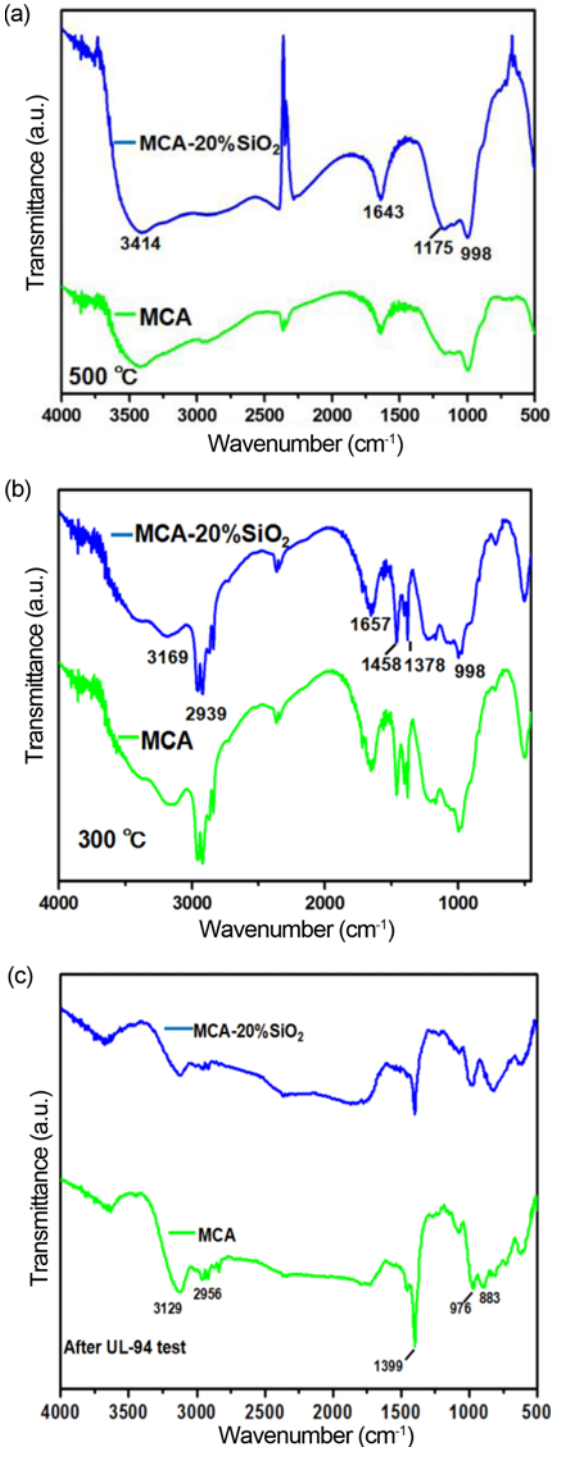

Figure 12. FTIR spectra of the composites at (a) 300 °C, (b) 500 °C, and (c) after combustion.

Figure 12(b) presents the FT-IR curves of the residue char of the samples at 500 °C. Compared to the FT-IR curves at 300 °C, the -OH bond (3169 cm^{-1}) was narrower, while -NH bonds at 414 cm^{-1} has a strong absorption, which indicated the dehydration reaction occurred in APP. In addition, when the temperature increased to 500 °C, the peaks of -CH$_2$ bonds at 1458, and 1378 cm^{-1} disappeared in the FT-IR spectra, which was attributed to the thermal degradation of PEPA. Peaks at 1175 and 952 cm^{-1} are attributed to the P-O-C bond and P=O bond streching, respectively. It was noted that the cross-linking reaction occurred between PEPA and phosphoric acid at the temperature range of 300-500 °C.

Figure 12(c) shows the FT-IR curves of the residue char of the composites after the UL-94 test. The peaks at 3129 cm^{-1} was assigned to the stretching vibration of the -OH bonds. Compared with the Figure 11(a) and Figure 11(b), it can be found that the bond of -C=N, -C=O (1657 cm^{-1}) became weaker and the new peaks occured at 1399 cm^{-1}, which was attributed to the degradation of MCA and the formation of the P-N bonds. The peaks at 976 cm^{-1} and 883 cm^{-1} were assigned to the P-O-C structure. Because the amount of added fumed silica was rather low, the absorption of Si-O bond [33,34] was not obvious or might be overlapped by other peaks.

In the process of GF-PP/IFR composites burning, which IFR were comprised of APP, PEPA and MCA or MCA-SiO$_2$, the schematic diagram explaining the char-forming mechanism was shown in Figure 13(a). it was proposed that the some representative chemical reactions occured in the char-forming process according to the infrared spectrum analysis above, which were depicted in Figure 13(b). First of all, APP was decomposed to form some polyphosphoric acid, which could catalyze the dehydration of GF-PP, APP, PEPA, MCA and SiO$_2$ molecules to form a cross-linked char layer to protect the underlying material. Among them, the hydroxyl groups on the surface of SiO$_2$ reacted with the hydroxyl groups on the surface of glass fiber through dehydration reaction to prevent the fuel flowing on the surface of GF. Meanwhile, the fumed silica nanoparticles with low thermal

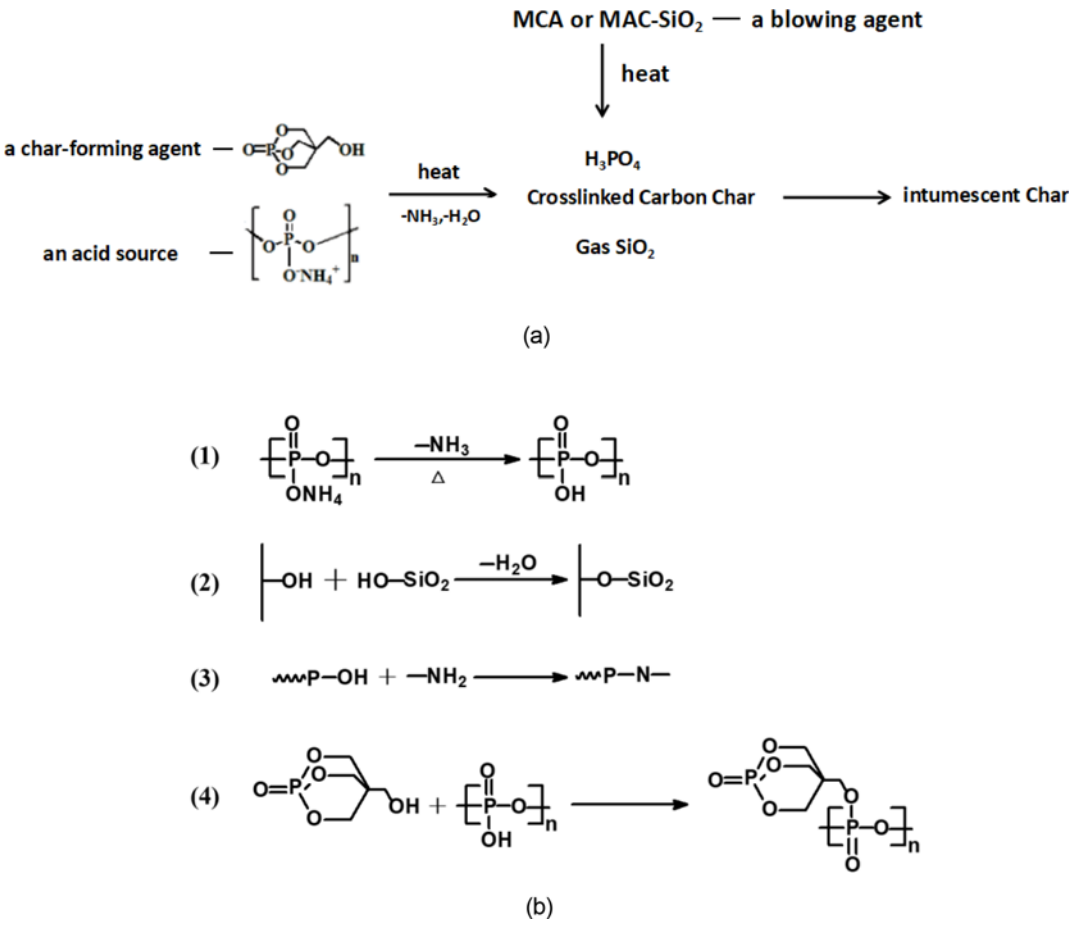

Figure 13. The schematic diagram explaining the fire retardant mechanism; (a) the schematic diagram explaining the char-forming mechanism and (b) possible reaction mechanism of GF-PP/IFR-(MCA-SiO_2) composites during burning.

conductivity coefficient effectively prevented the heat exchange, and make the char layer of the GF-PP/IFR-MCA samples more uniform and compact, leading to a reduction of the heat release of the material combustion and improvement of the flame retardant properties.

Conclusion

A new type of synergistic agent, MCA-SiO_2, were designed and synthesized by self-assembly of ME and CA in a suspension of the fumed silica. The fumed silica inhibited the formation of the hydrogen bonds between the acid and melamine, which contributed to the production of smaller particles of MCA. GF-PP/IFR-(MCA-SiO_2) composites were prepared by melting blend of GF-PP and IFR containing MCA-SiO_2. When the added amount of SiO_2 in MCA-SiO_2 system was 20 wt%, the flame retardant property of the GF-PP/IFR-(MCA-SiO_2) composites reached the UL-94 V-0 rating with a limiting oxygen index (LOI) of 32.4 %. The fumed silica reduced the heat release of the material combustion and improved the flame retardant properties of the material. The flame retardant mechanism was based on the low thermal conductivity of the fumed silica, which effectively prevented the heat exchange, and formed more uniform and compact char layer on the GF-PP/IFR-(MCA-SiO_2) composites in combustion to improve the flame retardant properties.

Acknowledgments

The authors appreciate the financial supports from Guangdong winner High-Tec & Industry Co. Ltd. and Municipal Bureau of science and technology of Foshan, Guangdong Province, China.

References

1. M. Sano, H. Oguma, M. Sekine, and C. Sato, *Int. J. Adhes. Adhes.*, **47**, 57 (2013).
2. T. Mohan and K. Kanny, *J. Reinf. Plast. Comp.*, **30**, 152 (2011).
3. M. Stevens and P. Coutelen, *ACS Sym. Ser.*, **1118**, 481

(2012).
4. Y. Liu, C. L. Deng, J. Zhao, J. S. Wang, and L. Chen, *Polym. Degrad. Stabil.,* **96**, 363 (2011).
5. S. Chen, J. Li, Y. Zhu, Z. Guo, and S. Su, *J. Mater. Chem. A.,* **1**, 15242 (2013).
6. B. Li and M. Xu, *Polym. Degrad. Stabil.,* **91**, 1380 (2006).
7. B. Yu, X. Wang, X. Qian, W. Xing, and H. Yang, *RSC Adv.,* **4**, 31782 (2014).
8. X. Y. Li, S. W. Tang, X. Q. Zhou, S. H. Gu, K. Huang, J. J. Xu, X. Wang, and Y. Li, *J. Appl. Polym. Sci*., **134**, 449 (2017).
9. J. J. Wang, L. Wang, and A. G. Xiao, *J. Macromol. Sci.: Part D-Rev.,* **48**, 297 (2009).
10. J. Huang, M. Liang, C. Feng, and H. Liu, *Polym. Eng. Sci.,* **56**, 380 (2016).
11. D. D. Yang, Y. Hu, H. T. Li, L. Song, H. P. Xu, and B. Li, *J. Therm. Anal. Calorim*., **119**, 619 (2015).
12. Y. Sheng, Y. H. Chen, and Y. Z. Bai, *Polym. Comp.,* **35**, 2390 (2014).
13. K. Q. Zhou, S. H. Jiang, B. B. Wang, Y. Q. Shi, J. J. Liu, N. N. Hong, Y. Hu, and Z. Gui, *Polym. Adv. Technol.,* **25**, 701 (2014).
14. Y. Liu, C. L. Deng, J. Zhao, J. S. Wang, L. Chen, and Y. Z. Wang, *Polym. Degrad. Stabil.,* **96**, 363 (2011).
15. Y. Y. Li, K. Liu, and R. Xiao, *Macromol. Res.,* **25**, 1 (2017).
16. Y. Y. Li, Y. Z. Lin, K. Sha, and R. Xiao, *Text. Res. J.,* **87**, 561 (2017).
17. Y. Liu and Q. Wang, *J. Polym. Res*., **16**, 583 (2009).
18. K. D. Li, J. Y. Xu, and J. Liu, *Acta Materiae Compositae Sinica*, **32**, 712 (2015).
19. S. S. Wei, L. Y. Wang, C. Liu, M. L. Yu, X. H. Chen, and X. D. Chen, *J. Nanosci. Nanotechnol*., **16**, 9919 (2016).
20. K. Sha, Y. L. Hu, Y. H. Wang, and R. Xiao, *Mater. Res. Innov*., **18**, 843 (2014).
21. X. L. Chen, Y. F. Jiang, J. B. Liu, C. M. Jiao, Y. Qian, and S. X. Li, *J. Therm. Anal. Calorim*., **120**, 1493 (2015).
22. J. Courtat, F. Melis, J. M. Taulemesse, V. Bounor-Legare, R. Sonnier, L. Ferry, and P. Cassagnau, *Polym. Degrad. Stabil*., **119**, 260 (2015).
23. L. Li and G. Yang, *J. Appl. Polym. Sci*., **115**, 3376 (2010).
24. Y. Y. Li, Y. Z. Lin, K. Sha, and R. Xiao, *Text. Res. J.,* **87**, 561 (2017).
25. M. Z. Fu and B. J. Qu, *Polym. Degrad. Stabil.,* **85**, 633 (2004).
26. Y. Liu and Q. Wang, *Polym. Eng. Sci.,* **20**, 220 (2004).
27. K. D. Li, J. Y. Xu, and J. Liu, *Acta Materiae Compositae Sinica*., **32**, 712 (2015).
28. C. M. Feng, Y. Zhang, S. W. Liu, Z. G. Chi, and J. R. Xu, *Polym. Adv. Technol*., **24**, 478 (2013).
29. K. Yang, M. J. Xu, and B. Li, *Polym. Degrad. Stabil.,* **98**, 1397 (2013).
30. C. M. Jiao and X. L. Chen, *J. Appl. Polym. Sci*., **120**, 1285 (2011).
31. S. Zhou, L. Song, Z. Z. Wang, Y. Hu, and W. Y. Xing, *Polym. Degrad. Stabil.,* **93**, 1799 (2008).
32. J. Liu and J. Y. Xu, *Plast*, **42**, 18 (2013).
33. S. P. Tong and D. P. Zhang, "Proceedings of 2008 National Flame Retardant Academic Conference", pp.145-152, Yichang Hubei China, May 18th, 2008.
34. Y. J. Chen, J. Zhan, P. Zhang, S. B. Nie, H. D. Lu, L. Song, and Y. Hu, *Ind. Eng. Chem. Res*., **49**, 8200 (2010).